Carbon 159 (2020) 611–616

Contents lists available at ScienceDirect

Carbon

journal homepage: www.elsevier.com/locate/carbon

Activation of graphitic nitrogen sites for boosting oxygen reduction

Guojie Chao [a], Longsheng Zhang [b, **], Dong Wang [a], Shan Chen [a], Hele Guo [a], Kaibing Xu [a], Wei Fan [a], Tianxi Liu [a, c, *]

[a] State Key Laboratory for Modification of Chemical Fibers and Polymer Materials College of Materials Science and Engineering, Innovation Center for Textile Science and Technology, Donghua University, Shanghai, 201620, China
[b] State Key Laboratory of Molecular Engineering of Polymers, Department of Macromolecular Science and Laboratory of Advanced Materials, Fudan University, Shanghai, 200438, China
[c] Key Laboratory of Synthetic and Biological Colloids, Ministry of Education, School of Chemical and Material Engineering, Jiangnan University, Wuxi, 214122, China

ARTICLE INFO

Article history:
Received 2 October 2019
Received in revised form
5 December 2019
Accepted 21 December 2019
Available online 23 December 2019

Keywords:
Carbon
Doping
Electrolysis
Active sites
Oxygen reduction

ABSTRACT

Carbon materials doped with sulfur (S) and nitrogen (N) are prospective alternatives to Pt-based catalysts as oxygen reduction reaction (ORR) catalyst since they are inexpensive and highly catalytic active. However, the further advancement of catalysts is greatly hindered for its unclear and equivocal catalytic sites. Here, using density functional theory studies, we find that those inactive carbon atoms next to graphitic N become ORR catalytic sites after S doping, which is distinctly different from N-doped carbon materials where catalytic sites are introduced by pyridinic N. The electrochemical results show that increasing the content of graphitic N can lead to higher catalytic activity for S and N dual-doped carbon materials, which exhibits higher turnover frequency towards ORR than that of N-doped carbon materials. This work provides insights for further advancement of electrocatalysts *via* heteroatom doping.

1. Introduction

Oxygen reduction reaction (ORR) is significant in various applications, especially in metal-air batteries, fuel cells and water purification [1–5]. The poor durability and high cost of currently-used Pt/C catalyst severely hinder the realistic viability of these applications [6,7]. With good catalytic performance and durability, cost-effective nitrogen (N)-doped carbon materials are supposed to replace Pt-based materials as ORR catalysts [8,9]. The ORR active sites in the N-doped carbon materials were recently determined as carbon atoms nearby pyridinic N sites [10]. Thus, it is an effective strategy to increase the content of pyridinic N and lower the content of inactive N species for improving the ORR performance. Nevertheless, the improvement is still limited, due to low intrinsic catalytic activity created by pyridinic N sites and the inevitable co-existence of different configurations of nitrogen species in N-doped carbon materials.

Previous studies have suggested that introducing another heteroatom (e.g., S, P and B) into N-doped carbon materials can enable the synergistic effects between the dopants and achieve enhanced ORR activity [11–16]. For S and N co-doped carbon materials, S atoms with close electronegativity to C atoms by virtue of its featuring *p* orbits, can cause the polarization of neighboring C or N atoms and create distinct matching electronic structure with N atoms [12,17,18]. As a result, the spin densities of C atoms adjacent to the S atoms can appreciably increase, leading to improved ORR activity. However, it remains uncharted how the S dopants interact with different types of N species in the S and N dual-doped carbon materials. The ORR active site(s) is still indistinct, which greatly limits farther advancement in catalyst design.

Herein, we further develop physical models and explore the ORR active sites in the S and N dual-doped carbon materials. Using density functional theory (DFT) studies, we find that inactive carbon atoms next to graphitic N become ORR active sites after S doping, which is different from N-doped carbon materials where active sites are created by pyridinic N. To experimentally verify the

* Corresponding author. State Key Laboratory for Modification of Chemical Fibers and Polymer Materials College of Materials Science and Engineering, Innovation Center for Textile Science and Technology, Donghua University, Shanghai, 201620, China.
** Corresponding author.
E-mail addresses: lszhang16@fudan.edu.cn (L. Zhang), txliu@dhu.edu.cn, txliu@fudan.edu.cn (T. Liu).

https://doi.org/10.1016/j.carbon.2019.12.052
0008-6223/

DFT calculations, we synthesized S and N dual-doped carbon nanosheets (SNC) with various contents of graphitic N, and N-doped carbon nanosheets (NC) as control. The electrochemical results manifest that increasing the content of graphitic N can lead to higher ORR activity for the SNC catalyst, which exhibits 1.6-times higher turnover frequency towards ORR than that of NC catalyst. The resultant SNC catalyst with high catalytic activity, good stability and methanol tolerance shows great potential as alternative ORR catalysts.

2. Experimental section

2.1. Synthesis of sulfur spheres

The sulfur (S) spheres were obtained by a modified method. First, 6.32 g $Na_2S_2O_3$ was dissolved into PVP aqueous solution (500 mL, 1 wt%) under magnetic stirring at room temperature. Then, 10 mL HCl aqueous solution (1 M) was dropwise added into the above solution under stirring. The mixture solution became turbidity after 10 min and became milky after 2 h. The precipitate (S spheres) was collected *via* centrifugation and vacuum drying.

2.2. Synthesis of SNC and NC catalysts

First, S spheres (1 g) were dispersed into tris(hydroxymethyl) aminomethane aqueous solution (0.1 M, 100 mL) by ultrasonication and the pH of the mixture was adjusted to 8.5. Then, 1 g of dopamine (DA) hydrochloride was added into the above solution. After 12 h stirring, the precipitate (PDA/S spheres) was collected *via* centrifugation and vacuum drying. Finally, the PDA/S spheres (100 mg) and urea (5 g) were mixed and heated at 1100 °C in Ar atmosphere for 2 h with a ramping rate of 5 °C min^{-1}. The resultant product was labeled as SNC. As control, the sample prepared *via* the same procedure without adding S spheres was labeled as NC. Besides, SNC-2, SNC-3 and SNC-4 samples with different contents of graphitic N were also synthesized *via* heating the mixture of PDA/S spheres (100 mg) and urea (5 g) at 1000 °C, 900 °C and 800 °C in Ar atmosphere for 2 h with a heating rate of 5 °C min^{-1}.

2.3. Electrochemical measurements

Electrochemical measurements were conducted using a three-electrode configuration with an electrochemical workstation (CHI 660D). The graphite rod and Ag/AgCl electrode (with saturated KCl as the filling solution) were employed as counter and reference electrodes, respectively. Typically, the catalyst powder (5 mg) was dispersed in a mixed solution with 0.35 mL of ethyl alcohol and 95 μL of Nafion solution (5 wt%) with ultrasonication to produce a homogeneous suspension. Then, working electrode was prepared by coating the glassy carbon electrode (GCE, diameter: 5 mm) with the catalyst suspension (5 μL).

Cyclic voltammetry (CV) was measured in 0.1 M KOH aqueous solution with a scan rate of 50 mV s^{-1} from −1.0 to +0.2 V (*vs.* Ag/AgCl). Linear sweep voltammetry (LSV) was recorded by employing the rotating disk electrode (RDE, Pine AFMSRCE 2762) technique. LSV tests were measured at various rotating speeds from 800 to 2400 rpm in O_2-saturated 0.1 M KOH with a scan rate of 10 mV s^{-1}. For rotating ring disk electrode (RRDE) tests, the disk electrode was scanned widely at a rate of 10 mV s^{-1} and the potential of ring electrode was set to 1.20 V *vs.* RHE (see details in supporting information).

3. Result and discussion

The electronic property of S-doped, N-doped as well as S and N co-doped graphene models were investigated using DFT calculations (see supporting information for the calculation details), with an aim to reveal the active sites. As reported, both charge density and spin density can work as a criterion to evaluate whether an atom is active site towards ORR, and spin density is a more important factor [19,20]. S atom has similar electronegativity to C atom and does not introduce extra unpaired electrons, hence the S-doped graphene model shows no spin density (Fig. S1) [18]. For N-doped graphene models (Fig. S2), four types of N dopants including pyridinic N, graphitic N, pyrrolic N and oxidized pyridinic N were considered. It is worthy to note that the spin density of carbon atoms remains unchanged for pyrrolic N or graphitic N doped graphene, while obvious enhancement is observed for pyridinic N and oxidized pyridinic N doped graphene. After further introducing S atom into these four N-doped graphene models with different positions between S and N atoms (Figs. S3–S6), we find that the spin densities of carbon atoms increase in the S, pyrrolic N co-doped graphene and S, graphitic N co-doped graphene models. Notably, the S, graphitic N co-doped graphene model features the highest spin density of carbon atoms. In the four-electron pathway towards ORR, desorption of *OOH intermediate is determined as the rate-determining step. As shown in Fig. S7, the *OOH intermediate prefers energetically to adsorb on the carbon atoms with higher spin density. Note that the O–OH bond of OOH intermediate is elongated from 1.343 Å to 1.417 Å when it is adsorbed on carbon atom, which will facilitate the breakage of O–OH bond. As indicated in Fig. 1, the spin density of carbon atoms greatly increases after S doping, with the highest spin density located at the C2 atom, which indicates that inactive carbon atoms next to graphitic N become active sites towards ORR [20]. These results indicate that co-doping of S and N heteroatoms not only increases the catalytic activity, but also governs the ORR active sites.

Inspired by DFT calculation results, we synthesized S and N co-doped carbon (SNC) materials with satisfactory content of N and S dopants. It was reported that porous and nanostructured materials with high accessible surface area would achieve better ORR activity. As illustrated in Fig. 2a, sulfur spheres wrapped by a thin layer of dopamine were first prepared (Fig. 2b and Fig. S8). Then the resultant sulfur/dopamine core/shell spheres were carbonized with urea at 1100 °C to obtain SNC nanosheet with porous structure (Fig. 2c and d). The gas-phase sulfur during pyrolysis would enable the ready formation of porous feature and facilitate higher content of heteroatom doping owing to the permeation from core to dopamine shell. The graphitic N is possible to be derived from both dopamine and urea. During the calcination process, adding urea is employed to further increase the content of N element. The content of N element for SNC obtained by carbonization of dopamine with urea (3.8%) is higher than that of SNC obtained without urea (2.0%). Uniform distribution of S and N elements throughout the whole nanosheet of SNC is revealed in Fig. 2e. The (002) carbon diffraction peak of SNC sample is weaker compared with the NC sample (Fig. 2f), indicating its lower graphitization degree due to heteroatom doping into the carbon skeleton. Raman spectra (Fig. 2g) show that the I_D/I_G (intensity ratio of D band and G band) of SNC sample is higher than NC sample, which is attributed to the disorder in the nanostructure caused by heteroatom doping [21]. As shown in Fig. S9, the N_2 adsorption curves of NC and SNC samples both show type-IV adsorption curves, indicating the presence of micropores and mesopores. Besides, the SNC sample has larger Brunauer-Emmett-Teller (BET) specific surface area than NC sample, which can provide more active sites for ORR.

X-ray photoelectron spectroscopy (XPS) was further characterized to study the chemical nature of SNC and NC samples (Fig. 3 and Fig. S10). The oxygen species can be deconvoluted into three contributions (C=O, C–O–C and C–OH) in the high-resolution O 1s

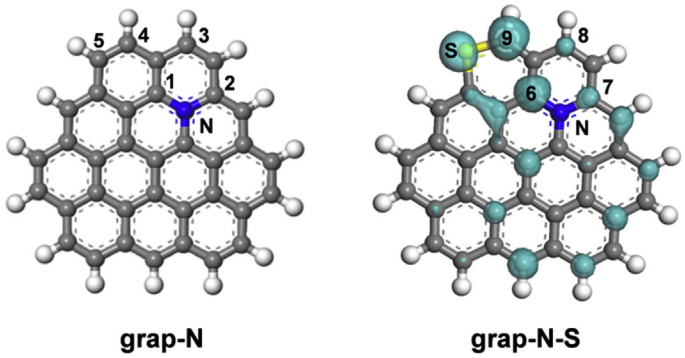

Atom	Spin Density	Atom	Spin Density
C1	0	C6	0.204
C2	0	C7	0.029
C3	0	C8	0.033
C4	0	C9	0.345
C5	0	S	0.146

Fig. 1. Spin density isosurface of graphitic N doped (gra-N) model and S, graphitic N co-doped (gra-N-S) graphene model. (A colour version of this figure can be viewed online.)

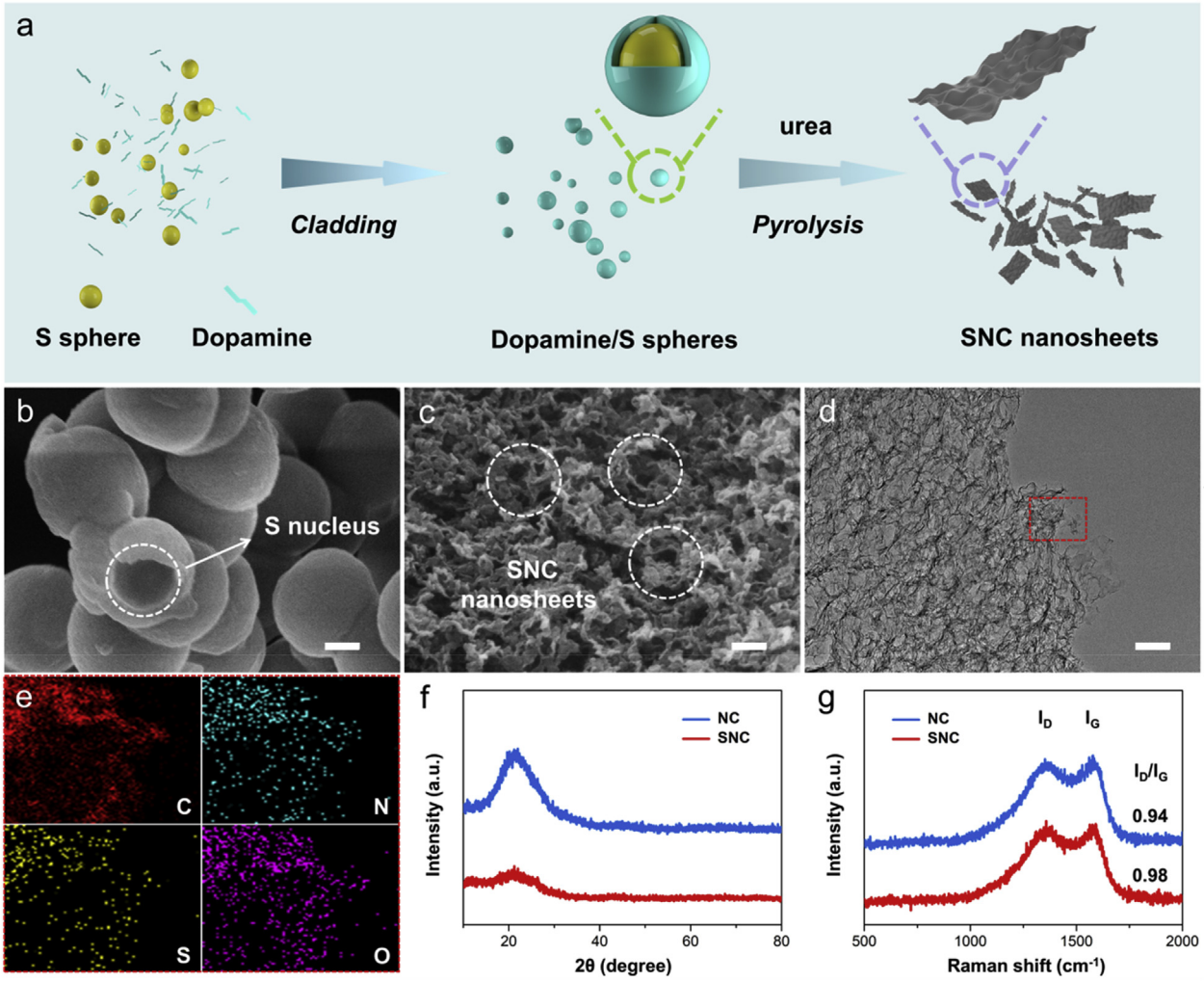

Fig. 2. (a) Illustration of synthesizing S and N dual-doped porous carbon (SNC) nanosheets. SEM images of the as-prepared (b) dopamine/S spheres and (c) SNC nanosheets. (d) TEM and (e) corresponding EDS mapping image of SNC nanosheets. Scale bar: 200 nm. (f) XRD patterns and (g) Raman spectra of the SNC and N-doped carbon (NC) nanosheets. Intensity ratio of D band to G band (I_D/I_G) is shown in (g). (A colour version of this figure can be viewed online.)

spectra (Fig. S11). The oxygen contents and species of NC and SNC samples are similar (Table S1 and Table S2), which is probably ascribed to the same calcination temperature during the preparation process. As displayed in Fig. 3a, the high-resolution spectra of N 1s were fitted into four peaks including pyridinic N (398.6 eV), pyrrolic N (400.5 eV), graphitic N (401.2 eV) and oxidized pyridinic N (402.0 eV) [11,22,23]. The content of different types of N species from XPS quantitative analysis are summarized in Fig. 3b and Table S1. It can be observed that the percentage of pyridinic N for the SNC sample is much lower than that of NC sample. The percentage of graphitic N for the SNC sample is markedly higher than that of NC sample. It is reported that the S atoms can substitute the edge carbon atoms of N-doped carbon skeleton, which would concomitantly influence the composition of N species [24]. The

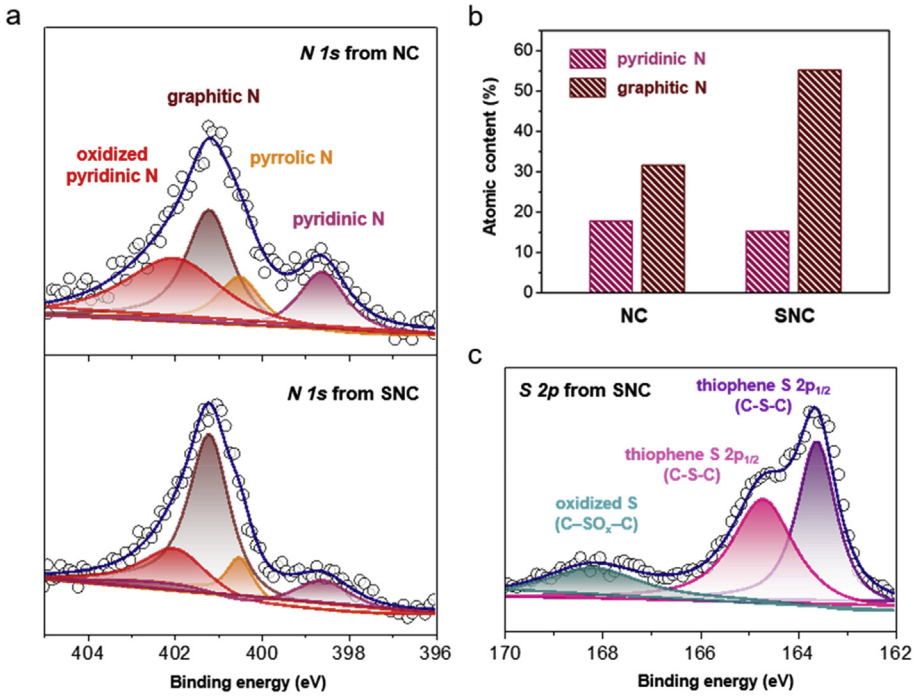

Fig. 3. (a) High-resolution N 1s spectra and (b) the atomic percentage of pyridinic N and graphitic N species for NC and SNC samples. (c) High-resolution S 2p spectrum of SNC sample. (A colour version of this figure can be viewed online.)

thermodynamic energy barriers for S atoms substituting the edge carbon and pyridinic N of N-doped carbon model is lower than that of S atoms substituting graphite N [24]. Thus the doping of S atoms would cause the different composition of N types for NC and SNC samples. The spectra of S 2p (Fig. 3c) were fitted into three peaks of thiophene S $2p_{3/2}$ (163.6 eV), thiophene S $2p_{1/2}$ (164.7 eV) and oxidized S (C-SO_X-C) (168.2eV) [25–27]. Notably, it is energetically difficult to form covalent bonds between S and N atoms due to the large distance between them [28]. As discussed in DFT studies, the carbon atoms next to graphitic N become ORR active sites for SNC samples, which suggests higher content of graphitic N would lead to higher ORR activity. Thus, SNC samples with different contents of graphitic N (Fig. S12, Fig. S13, Table S3 and Table S4) were also synthesized as control, to investigate the effect of the graphitic N content of samples on their catalytic activity.

To evaluate the ORR performance of SNC and NC samples, CV and LSV of catalysts deposited on GCEs were measured in O_2-saturated 0.1 M KOH aqueous electrolyte. From Fig. S14, characteristic reduction peaks are observed in the CV curves of both samples in O_2-saturated electrolyte, while no redox peaks are found in the N_2-saturated electrolyte. Notably, the potential of the reduction peak for SNC sample is much more positive than NC sample, indicating its higher catalytic activity towards ORR. The LSV curves reveal that the SNC sample exhibits a more positive half-wave potential ($E_{1/2}$) than NC sample (Fig. 4a). Specifically, the $E_{1/2}$ (0.83 V *vs.* RHE) of SNC sample is much higher than that (0.79 V *vs.* RHE) of NC sample, and even comparable with that (0.85 V vs. RHE) of commercial Pt/C catalyst. We have further compared the electrochemical performance of four SNC samples with different percentages of graphitic-N. As shown in Fig. S15, the half-wave potential ($E_{1/2}$) of these samples increases concomitantly as the percentage of graphitic N species of samples increases, which verifies the dependence of ORR catalytic activity on the graphitic N contents. Since the conductivities and morphologies of these four SNC samples may be different, we have further analyzed the electrochemical performance with currents *i*R-corrected and the specific activities of samples with currents normalized to the BET surface area, respectively. As shown in Fig. S16, the *i*R-corrected LSV curves show that the SNC sample exhibits a more positive half-wave potential than other samples, indicating its highest catalytic activity. As shown in Fig. S17, the LSV curves (with current normalized by BET surface area) indicate that the SNC sample exhibits highest ORR activity among all samples. In conjunction with the DFT results, the increased catalytic activity of SNC catalyst can be attributed to its increased content of graphitic N. With the conductivity and porous structure of samples considered, the activity trends still remain dependent on the graphitic N contents of samples. The SNC catalyst also exhibits higher catalytic activity than NC catalyst in acidic media (Fig. S18), which is in accordance with the activity trends measured in alkaline condition. As displayed in Fig. 4b and Fig. S19, the Tafel slope of SNC (98 mV dec^{-1}) is much lower than those of NC (117 mV dec^{-1}) and Pt/C (142 mV dec^{-1}), indicating its faster reaction kinetics.

In order to study the intrinsic activity of SNC and NC samples, we obtained their active site density (SD_m) using the double-layer capacitance (C_{dl}) method (Fig. S20) [29,30]. The SD_m of SNC sample (3.1×10^{20} sites g^{-1}) is greatly higher than that of NC sample (2.5×10^{20} sites g^{-1}). Besides, the turnover frequency (TOF) based on carbon atoms was then calculated to assess the intrinsic activity of every single site (Fig. 4c and Table S5). The TOF of SNC sample is 0.38×10^{-3} s^{-1}, which is much higher than that of NC sample (0.24×10^{-3} s^{-1}), indicating its enhanced intrinsic catalytic activity after S doping. The TOF is based on the mole number of carbon atoms on the electrode calculated *via* the total loading mass. The enhanced TOF of SNC catalyst is in accordance with the increased spin density of carbon atoms next to graphitic N after S doping (from DFT studies in Fig. 1). Furthermore, the electron transfer number and peroxide yield based on RRDE tests are also obtained (Fig. 4d and Fig. S21). With electron transfer number closer to four and much lower peroxide yield, the SNC sample demonstrates its

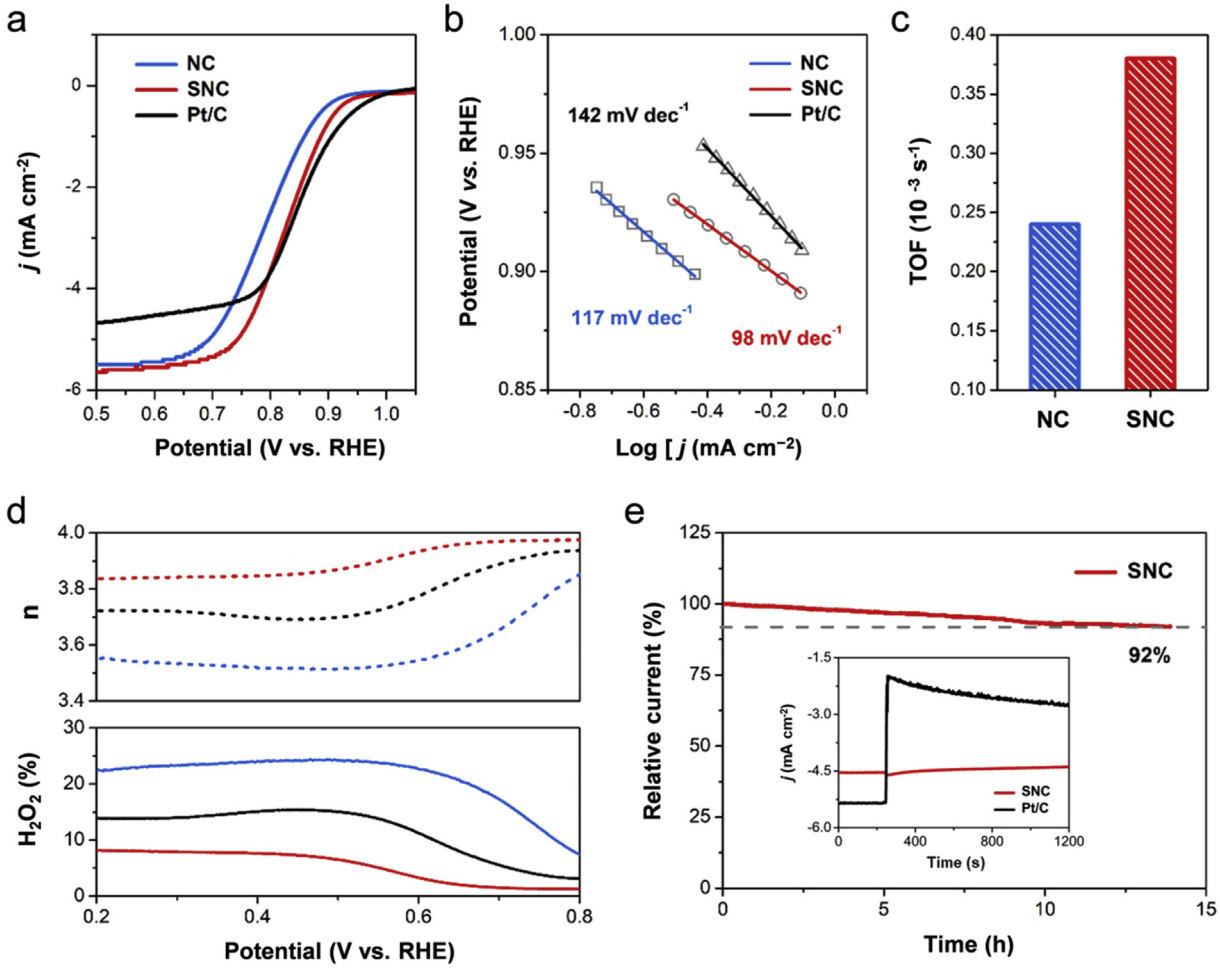

Fig. 4. (a) LSV curves of NC, SNC and commercial Pt/C catalysts on GCEs in O_2-saturated 0.1 M KOH aqueous electrolyte at a scan rate of 10 mV s^{-1}. (b) Tafel plots of NC, SNC and Pt/C catalysts. (c) Comparison of turnover frequency for the SNC and NC at 0.6 V (*vs.* RHE). (d) Electron transfer number (n) and peroxide (H_2O_2) yield for the NC (blue), SNC (red) and Pt/C (black) catalysts. (e) Stability evaluation of SNC catalyst at 0.71 V (vs. RHE), and *i*-t curves of SNC and Pt/C catalysts with addition of 1 M methanol (inset of e). (A colour version of this figure can be viewed online.)

higher catalytic efficiency and selectivity than the NC sample [31,32]. The electron transfer numbers calculated from the Koutecky-Levich plots of SNC sample at different potentials are all near 4 (Fig. S22), indicating its stable four-electron ORR process.

Aside from intrinsic catalytic activity and selectivity, long-term stability and methanol tolerance are also crucial factors of ORR catalysts. As displayed in Fig. 4e, the SNC catalyst exhibits good stability with negligible loss (8%) over 14 h. Besides, when exposed to methanol, the SNC sample remains very stable while the commercial Pt/C catalyst undergoes a sharp current decline (inset of Fig. 4e). High catalytic activity, good stability and methanol tolerance, along with the cost-effective property of SNC catalyst, make it prospective alternatives to Pt-based ORR catalysts.

4. Conclusions

In summary, we demonstrate that the inactive carbon atoms next to graphitic N become ORR active sites after S doping, as verified by the DFT calculations and experimental results. The active sites of S and N co-doped carbon materials are different from N-doped carbon materials where active sites are introduced by pyridinic N. The co-doping of S and N heteroatoms not only increases the intrinsic catalytic activity and selectivity, but also governs the active sites. This work provides insights for further advancement of electrocatalysts *via* heteroatom doping.

Author contributions

T.X.L. and L.S.Z. supervised the project. G.J.C., L.S.Z., and W.F. designed and carried out the experiments. D.W., S.C., H.L.G. and K.B.X assisted in the experiments. G.J.C., L.S.Z., W.F. and T.X.L. wrote the manuscript. All authors discussed the results and assisted during manuscript preparation.

Declaration of competing interest

The authors declare no competing financial interest.

Acknowledgements

The authors are grateful for the financial support from the National Natural Science Foundation of China (21704014, 51433001), the Fundamental Research Funds for the Central Universities (2232017D-06, 2232019A3-03), Shanghai Municipal Education Commission (17CG33), Program of Shanghai Academic Research Leader (17XD1400100), Shanghai Sailing Program (17YF1400200), and Shanghai Scientific and Technological Innovation Project (18JC1410600).

Appendix A. Supplementary data

Supplementary data to this article can be found online at https://doi.org/10.1016/j.carbon.2019.12.052.

References

[1] M.K. Debe, Electrocatalyst approaches and challenges for automotive fuel cells, Nature 486 (2012) 43–51.
[2] L. Chong, J.G. Wen, J. Kubal, F.G. Sen, J.X. Zou, J. Greeley, et al., Ultralow-loading platinum-cobalt fuel cell catalysts derived from imidazolate frameworks, Science 362 (2018) 1276–1281.
[3] H.J. Shen, E. Gracia-Espino, J.Y. Ma, K.T. Zang, J. Luo, L. Wang, et al., Synergistic effects between atomically dispersed Fe-N-C and C-S-C for the oxygen reduction reaction in acidic media, Angew. Chem. Int. Ed. 56 (2017) 13800–13804.
[4] N. Zhang, Y.G. Feng, X. Zhu, S.J. Guo, J. Guo, X.Q. Huang, Superior bifunctional liquid fuel oxidation and oxygen reduction electrocatalysis enabled by PtNiPd core-shell nanowires, Adv. Mater. 29 (2017), 1603774.
[5] S.C. Chen, Z.H. Chen, S. Siahrostami, D. Higgins, D. Nordlund, D. Sokaras, et al., Designing boron nitride islands in carbon materials for efficient electrochemical synthesis of hydrogen peroxide, J. Am. Chem. Soc. 140 (2018) 7851–7859.
[6] X.X. Wang, M.T. Swihart, G. Wu, Achievements, challenges and perspectives on cathode catalysts in proton exchange membrane fuel cells for transportation, Nat. Catal. 2 (2019) 578–589.
[7] H.T. Chung, D.A. Cullen, D. Higgins, B.T. Sneed, E.F. Holby, K.L. More, et al., Direct atomic-level insight into the active sites of a high-performance PGM-free ORR catalyst, Science 357 (2017) 479–483.
[8] K.P. Gong, F. Du, Z.H. Xia, M. Durstock, L.M. Dai, Nitrogen-doped carbon nanotube arrays with high electrocatalytic activity for oxygen reduction, Science 323 (2009) 760–764.
[9] L.T. Qu, Y. Liu, J.B. Baek, L.M. Dai, Nitrogen-doped graphene as efficient metal-free electrocatalyst for oxygen reduction in fuel cells, ACS Nano 4 (2010) 1321–1326.
[10] D.H. Guo, R. Shibuya, C. Akiba, S. Saji, T. Kondo, J. Nakamura, Active sites of nitrogen-doped carbon materials for oxygen reduction reaction clarified using model catalysts, Science 351 (2016) 361–365.
[11] J. Liang, Y. Jiao, M. Jaroniec, S.Z. Qiao, Sulfur and nitrogen dual-doped mesoporous graphene electrocatalyst for oxygen reduction with synergistically enhanced performance, Angew. Chem. Int. Ed. 51 (2012) 11496–11500.
[12] J.J. Li, Y.M. Zhang, X.H. Zhang, J.Z. Huang, J.C. Han, Z.H. Zhang, et al., S, N dual-doped graphene-like carbon nanosheets as efficient oxygen reduction reaction electrocatalysts, ACS Appl. Mater. Interfaces 9 (2017) 398–405.
[13] J.T. Zhang, Z.H. Zhao, Z.H. Xia, L.M. Dai, A metal-free bifunctional electrocatalyst for oxygen reduction and oxygen evolution reactions, Nat. Nanotechnol. 10 (2015) 444–452.
[14] T. Sun, J. Wang, C.T. Qiu, X. Ling, B.B. Tian, W. Chen, et al., B, N co-doped and defect-rich nanocarbon material as a metal-free bifunctional electrocatalyst for oxygen reduction and evolution reactions, Adv. Sci. 5 (2018), 1800416.
[15] S. Zhao, Y.W. Zhang, Y.M. Zhou, Y.Y. Wang, K.B. Qiu, C. Zhang, et al., Facile one-step synthesis of hollow mesoporous g-C_3N_4 spheres with ultrathin nanosheets for photo-redox water splitting, Carbon 126 (2018) 247–256.
[16] W. Yang, W. Yang, L.N. Kong, A.L. Song, X.J. Qin, G.J. Shao, Phosphorus-doped 3D hierarchical porous carbon for high-performance supercapacitors: a balanced strategy for pore structure and chemical composition, Carbon 127 (2018) 557–567.
[17] D.S. Yang, D. Bhattacharjya, S. Inamdar, J. Park, J.S. Yu, Phosphorus-doped ordered mesoporous carbons with different lengths as efficient metal-free electrocatalysts for oxygen reduction reaction in alkaline media, J. Am. Chem. Soc. 134 (2012) 16127–16130.
[18] L.P. Zhang, J.B. Niu, M.T. Li, Z.H. Xia, Catalytic mechanisms of sulfur-doped graphene as efficient oxygen reduction reaction catalysts for fuel cells, J. Phys. Chem. C 118 (2014) 3545–3553.
[19] Y.W. Liu, C. Xiao, P.C. Huang, M. Cheng, Y. Xie, Regulating the charge and spin ordering of two-dimensional ultrathin solids for electrocatalytic water splitting, Chem 4 (2018) 1263–1283.
[20] L.P. Zhang, Z.H. Xia, Mechanisms of oxygen reduction reaction on nitrogen-doped graphene for fuel cells, J. Phys. Chem. C 115 (2011) 11170–11176.
[21] I.M. Sundaram, S. Kalimuthu, G. Ponniah, Highly active ZnO modified g-C_3N_4 nanocomposite for dye degradation under UV and visible light with enhanced stability and antimicrobial activity, Compos. Commun. 5 (2017) 64–71.
[22] S.B. Yang, L.J. Zhi, K. Tang, X.L. Feng, J. Maier, K. Mullen, Efficient synthesis of heteroatom (N or S)-doped graphene based on ultrathin graphene oxide-porous silica sheets for oxygen reduction reactions, Adv. Funct. Mater. 22 (2012) 3634–3640.
[23] Z.Y. Lu, B.F. Wang, Y.F. Hu, W. Liu, Y.F. Zhao, R.O. Yang, , et al.Sun, An isolated zinc-cobalt atomic pair for highly active and durable oxygen reduction, Angew. Chem. Int. Ed. 58 (2019) 2622–2626.
[24] J.C. Li, X.P. Qin, P.X. Hou, M. Cheng, C. Shi, C. Liu, H.M. Cheng, M.H. Shao, Identification of active sites in nitrogen and sulfur co-doped carbon-based oxygen reduction catalysts, Carbon 147 (2019) 303–311.
[25] Z.X. Wu, R. Liu, J. Wang, J. Zhu, W.P. Xiao, C.J. Xuan, et al., Nitrogen and sulfur co-doping of 3D hollow-structured carbon spheres as an efficient and stable metal free catalyst for the oxygen reduction reaction, Nanoscale 8 (2016) 19086–19092.
[26] M. Klingele, C. Pham, K.R. Vuyyuru, B. Britton, S. Holdcroft, A. Fischer, et al., Sulfur doped reduced graphene oxide as metal-free catalyst for the oxygen reduction reaction in anion and proton exchange fuel cells, Electrochem. Commun. 77 (2017) 71–75.
[27] B.B. Huang, Y.C. Liu, X. Huang, Z.L. Xie, Multiple heteroatom-doped few-layer carbons for the electrochemical oxygen reduction reaction, J. Mater. Chem. A 6 (2018) 22277–22286.
[28] L.J. Zhai, Y.L. Sun, J.J. Yang, H.C. Wang, Z.P. Li, M.R. Xia, F.M. Gao, J. Wang, Moderate adsorption of oxygen molecular induced better performance of oxygen reduction reaction, Appl. Catal., B 166 (2019) F386–F392.
[29] A. Chakraborty, R. Devivaraprasad, B. Bera, M. Neergat, Electrochemical estimation of the active site density on metal-free nitrogen-doped carbon using catechol as an adsorbate, Phys. Chem. Chem. Phys. 19 (2017) 25414–25422.
[30] F.L. Meng, H.X. Zhong, D. Bao, J.M. Yan, X.B. Zhang, In situ coupling of strung Co_4N and intertwined N-C fibers toward free-standing bifunctional cathode for robust, efficient, and flexible Zn air-batteries, J. Am. Chem. Soc. 138 (2016) 10226–10231.
[31] Y.E. Miao, F.L. Lai, H.Y. Lu, J.J. Yan, Y.P. Huang, T.X. Liu, Nanocubic-Co_3O_4 coupled with nitrogen-doped carbon nanofiber network: a synergistic binder-free catalyst toward oxygen reduction reactions, Compos. Commun. 1 (2016) 15–19.
[32] E.G. Luo, H. Zhang, X. Wang, L.Q. Gao, L.Y. Gong, T. Zhao, et al., Single-atom Cr-N-4 sites designed for durable oxygen reduction catalysis in acid media, Angew. Chem. Int. Ed. 58 (2019) 12469–12475.